Journal of *Marine Science and Engineering*

MDPI

Article

Research on Two-Phase Flow and Wear of Inlet Pipe Induced by Fluid Prewhirl in a Centrifugal Pump

Jilong Chen [1], Xing Chen [2], Wenjin Li [2], Yuhai Zheng [3] and Yi Li [1,*]

[1] Key Laboratory of Fluid Transmission Technology of Zhejiang Province, Zhejiang Sci-Tech University, Hangzhou 310018, China; chenjlzstu@163.com
[2] Kunming Jiahe Science & Technology Co., Ltd., Kunming 650501, China; chenxing@jhpumps.com (X.C.); liwenjin@jhpumps.com (W.L.)
[3] Zhejiang Institute of Mechanical & Electrical Engineering, Co., Ltd., Hangzhou 310051, China; zhengyuhai_zjimee@outlook.com
* Correspondence: liyi@zstu.edu.cn

Abstract: In deep-sea mining hydraulic lifting systems, centrifugal pumps are very important as power units. In the process of transportation, the fluid prewhirl phenomenon in the impeller inlet will lead to changes in the state of motion of the particles and fluid and cause the wear of the inlet pipe, which can lead to centrifugal pump failure in serious cases. In this paper, a numerical simulation of the centrifugal pump is carried out based on the CFD-DEM coupling method to analyze the influence of the prewhirl on the wear of the inlet pipe. The results show that the velocity streamline near the impeller inlet position changes significantly. The flow field velocity increases along the radial direction of the inlet pipe, and it has a maximum value at r/R = 0.98. The prewhirl flow pulls the particles to change their original motion direction, and the area where the particles are subjected to high fluid force is concentrated between 0.5 d/D and 1 d/D, about 0.015 to 0.018 N, resulting in the uneven distribution of particles. The high-wear area appears in the bottom-left area (specifically, L4, L9, and L13), and this is also the location of the largest cumulative force; the high-wear area shows a triangle. The collision energy loss of particles increases due to the influence of the prewhirl, which leads to an increase in wear.

Keywords: centrifugal pump; inlet pipe; CFD-DEM; prewhirl; wear

Citation: Chen, J.; Chen, X.; Li, W.; Zheng, Y.; Li, Y. Research on Two-Phase Flow and Wear of Inlet Pipe Induced by Fluid Prewhirl in a Centrifugal Pump. *J. Mar. Sci. Eng.* **2024**, *12*, 950. https://doi.org/10.3390/jmse12060950

Academic Editor: Decheng Wan

Received: 24 April 2024
Revised: 25 May 2024
Accepted: 29 May 2024
Published: 5 June 2024

1. Introduction

In deep-sea mining projects, minerals from the seafloor, such as polymetallic manganese nodules, need to be lifted to mining platforms or vessels on the surface. In the hydraulic lifting system, centrifugal pumps are used to transport the mixture containing solid mineral particles to the surface through the lifting pipeline [1,2], and the performance and reliability of centrifugal pumps, which are the core power devices, are very important for safety [3].

Pump prewhirl is a phenomenon in which a fluid acquires a certain rotational motion before it enters the impeller of the pump. Yin et al. [4] found that the prewhirl phenomenon exists in the inlet pipe of a centrifugal pump, and CFD numerical simulations were carried out for this purpose at different flow rates. Chalghoum et al. [5] found that the prewhirl has a greater effect on the amplitude of pressure fluctuation when studying the effect of transient pressure fluctuation on the centrifugal pump's performance, and the stronger the prewhirl is, the greater the amplitude of the transient pressure is. Zhou et al. [6] studied the prewhirl and found that the appropriate positive prewhirl can improve the efficiency of the centrifugal pump. Huang et al. [7] researched the unsteady turbulent pressure fluctuations in a water jet propulsion system and found that the airflow in the conduit shows periodic prewhirl motion. Lu et al. [8] studied the noise caused by the unsteady flow through the numerical simulation of the pump. They found the prewhirl region caused

by the impeller rotation exhibits a spiraling circular motion. Yang et al. [9] researched the effect of positive prewhirl on the hydraulic performance of the pump under non-rated flow. The results showed that, under overloaded flow conditions, the prewhirl leads to an increase in the intensity of the flow, resulting in significant energy losses. However, most of the above studies were conducted on the basis of single-phase flow. In the study of solid–liquid two-phase flow fields, it is generally assumed that the inlet is a uniform incoming flow, and the effect of the presence of the prewhirl in the inlet flow field on the motion of particles is less considered. When a pump transports particle two-phase media, its performance and internal flow field will be different from those in clear water conditions. The particles will interact with the fluid during transportation in the pump, and the flow field characteristics will be changed. The particles will collide with the over-flow components, causing wear and tear on them, leading to performance degradation as well as the failure of the centrifugal pump [10–12]. The presence of the prewhirl phenomenon can lead to clogging and wear in the inlet pipe of centrifugal pumps with a two-phase flow of particles [13–16]. Thus, the study of two-phase flow and wear in the inlet pipe is necessary.

In terms of particle two-phase flow research methods, many scholars have used the CFD-DEM method to carry out their own studies. Li et al. [17] researched the flow in a bend with bumps in order to investigate the wear caused by particles on bends with different wall surfaces. The results show that the effect on the wear rate is most pronounced when the position of the bumps is close to the position of the first collision of the particles. Li et al. [18] investigated the wear of a two-phase flow with a normal distribution of the particle sizes in 90° bends using the CFD-DEM method and found that the particles form a protective layer. Tang et al. [19] used four types of polyhedral particles and one type of spherical particle to investigate the wear in pumps. They found that the wear suffered by the pump increases gradually with an increase in the degree of sphericity. Shi et al. [20] analyzed the flow field and particle trajectory of a pump with an optimized inlet structure. After an experimental comparison, it was found that the simulation model had good accuracy. Su et al. [21] studied the motion of large particles in a two-stage pump, and the results showed the method can accurately predict the pump performance curve obtained from experiments and, at the same time, analyze the particles at the impeller and the worm casing information, such as position distribution and velocity. Tan et al. [22] investigated the characteristics of non-spherical particles in a centrifugal pump. The results show that the cylindrical particles will move towards the pressure surface to form a pileup. Wang et al. [23] investigated the spatial distribution and kinematic properties of particles with different diameters in pumps. Li et al. [24] performed numerical simulations to study the changes in the motion of particles in a pump under different vibration conditions. They found the particle passage inside the centrifugal pump would be higher as the vibration frequency increased.

The above studies show that the CFD-DEM coupling method is reliable for a solid–liquid two-phase flow in centrifugal pump simulation. However, there is insufficient research on the prewhirl effect on particle motion characteristics in the inlet pipe. The effect of the prewhirl flow field on the particle motion will directly affect the wear position and wear degree of the flow passage wall. Therefore, based on the CFD-DEM coupling method, this paper investigates the influence of the impeller inlet prewhirl of the two-phase flow in the inlet pipe and the wear of the wall, and the results of our research can provide certain theoretical support for the design optimization of the solid–liquid mixing centrifugal pump.

2. Research Method

2.1. Numerical Method

In this paper, the CFD-DEM coupling method was used. The principle of the CFD-DEM coupling method lies in the fact that the liquid phase is computed in FLUENT 18.2 software and the solid phase is computed in EDEM 2018 software, and the data are exchanged at each time step. The FLUENT software will first perform a flow field calculation, and after the current time step has converged, the FLUENT software will pass

the velocity and pressure information to the EDEM software through the coupling interface, and the EDEM software will perform another time step. After convergence, it will pass the particle force information to the FLUENT software through the coupling interface, and the FLUENT software will perform another time step.

The basic governing equations for solving the liquid phase are as follows:

$$\nabla \cdot (\rho u) = 0 \tag{1}$$

$$\frac{\partial u}{\partial t} + u \cdot \nabla u = -\frac{1}{\rho_f}\nabla p + \nu \nabla^2 u + f_g + f_{fp} \tag{2}$$

where t is the time, ρ is the density of the fluid, u is the velocity of the fluid, p is the pressure of the fluid, and f_{fp} is the momentum exchange between the particles and the fluid.

The turbulence model used in this paper is the RNG k-ε model [25]. The model supplements the differential equations for turbulent kinetic energy and its dissipation rate to close the set of turbulent time-averaged control equations. Compared to the standard k-e model, the RNG k-ε model is a deformation of the standard model by correcting the turbulent viscosity, taking into account the rotation in the mean flow, and adding an extra term to the generation term in the equations to reflect the main flow time-averaged strain rate. Therefore, the RNG k-ε model can better handle flows with high strain rates and a large degree of streamline curvature. The equations of the RNG k-ε model are as follows:

$$\frac{\partial(\rho k)}{\partial t} + \frac{\partial(\rho k u_i)}{\partial x_i} = \frac{\partial}{\partial x_j}\left[\left(\mu + \frac{\mu_t}{\sigma_\varepsilon}\right)\frac{\partial k}{\partial x_j}\right] + G_k - \rho\varepsilon + S_k \tag{3}$$

$$\frac{\partial(\rho \varepsilon)}{\partial t} + \frac{\partial(\rho \varepsilon u_i)}{\partial x_i} = \frac{\partial}{\partial x_j}\left[\left(\mu + \frac{\mu_t}{\sigma_\varepsilon}\right)\frac{\partial \varepsilon}{\partial x_j}\right] + G_{1\varepsilon}^{*}\frac{\varepsilon}{k}G_k - G_{2\varepsilon}\rho\frac{\varepsilon^2}{k} + S_\varepsilon \tag{4}$$

$$\mu_t = \rho C_\mu \frac{k^2}{\varepsilon} \tag{5}$$

$$C_{1\varepsilon}^{*} = C_{1\varepsilon} - \frac{\eta\left(1 - \frac{\eta}{\eta_0}\right)}{1 + \beta\eta^3} \tag{6}$$

$$\eta = \left(2E_{ij}\cdot E_{ij}\right)^{\frac{1}{2}}\frac{k}{\varepsilon} \tag{7}$$

$$E_{ij} = \frac{1}{2}\left(\frac{\partial u_i}{\partial x_j} + \frac{\partial u_j}{\partial x_i}\right) \tag{8}$$

where $C_\mu = 0.0845$, $C_{1\varepsilon} = 1.42$, $C_{2\varepsilon} = 1.68$, $\eta_0 = 4.377$, $\beta = 0.012$.

The equations of control for the motion of particles in a flow field are described by Newton's second law. For the motion of particles in a flow field, the governing equations usually need to take into account the different forces acting on the particles. According to the characteristics of two-phase media in solid–liquid mixing pumping and piping systems, the main forces include gravity, the force of the fluid on the particles, and the force of the particles or the wall on the particles. The equations are expressed as follows:

$$m_p\frac{dV_p}{dt} = F_g + F_f + \sum F_c \tag{9}$$

$$I_p\frac{d\omega_p}{dt} = M_{ct} + M_{fp} \tag{10}$$

$$F_f = F_d + F_l + F_p + F_{am} + F_B \tag{11}$$

where V_p is the velocity of the particle, $\sum F_c$ is the sum of all contact forces on the particle with other particles or walls, F_g is the force of gravity, F_f is the force of fluid, I_p is the

particle rotational inertia, M_{ct} is the sum of the contact momentum of the particle with other particles in the flow field, ω_p is the angular velocity, M_{fp} is the momentum of resistance on the particle, F_d is the fluid resistance, F_l is the fluid lift force, F_B is the Basset force, F_{am} is the added mass force, and F_p is the pressure gradient force.

The contact forces between particles include normal and tangential forces; the Hertz–Mindlin contact model [26] is used. This is based on elastomer theory and is suitable for describing the contact force between hard particles, in which the particles are regarded as ideal elastic spheres, and the model treats the interactions between the particles as a spring and damping system, which is used to describe the elastic and damping forces between the particles. The model can be used to simulate particle–wall contact when one of the particles has an infinite particle size. The contact force equation is given below:

$$F_c = F_n + F_t \tag{12}$$

$$F_n = -k_n\delta_n - \eta_n v_n \tag{13}$$

$$F_t = -k_t\delta_t - \eta_t v_t \tag{14}$$

where F_n is the normal force; F_t is the tangential force; k_n and k_t denote the normal and tangential stiffness of the spring, respectively; δ_n and δ_t are the normal and tangential relative displacements between the particles or between the particles and the wall; η_n and η_t denote the normal and tangential damping coefficients, respectively; and v_n and v_t are the normal and tangential relative velocities between the particles or between the particles and the wall, respectively.

The Archard [27] wear model is used to calculate the wear:

$$Q = K\frac{WL}{H_v} \tag{15}$$

where Q is the wear volume, K is the dimensionless wear constant (take $K = 1 \times 10^{-11}$), L is the sliding distance, W is the applied load, and H_v is the hardness of the wall material.

The wall thickness loss h can be derived from the wear model:

$$h = \frac{K}{H_v A}WL \tag{16}$$

where A is the contact area.

2.2. Model and Mesh

The design parameters of the studied pump are as follows: a rated flow rate of 1200 m^3/h, a rated head of 95 m, a rated shaft power of 710 kW, and a rated efficiency of 79%. The speed of the pump is 990 rpm, the number of impellers is 5, the inlet diameter of the impeller is 350 mm, the maximum diameter of the impeller is 760 mm, and the outlet diameter of the volute is 260 mm. The geometric model is shown in Figure 1.

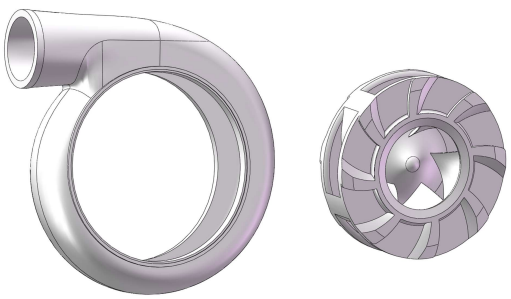

Figure 1. Geometric model.

The centrifugal pump is hydraulically modeled in the fluid domain. The main parts are the inlet pipe, the impeller, the volute, and the outlet pipe. The hydraulic model of the fluid domain is shown in Figure 2. The domain dimensions of the model are shown in Table 1. The hydrodynamic model is meshed with 6 sets of mesh, ranging from 2,352,531 to 7,652,523. Table 2 shows the mesh type of the model. The numerical simulation is carried out with the same boundary conditions, i.e., a flow rate of 1200 m^3/h, a rotational speed of 990 rpm, and water as the fluid medium. Among them, the inlet is set as a velocity inlet in FLUENT software (the velocity value is 3.465 m/s) and the outlet is set as an outflow in steady calculation. Figure 3 shows the results, and the head shows a trend of rising and then falling and then tends to level off. A grid number of 6,454,931 is finally selected, and the quality of this set of grids as well as the smallest angle meet the requirements of the calculation. Figure 4 shows the mesh model.

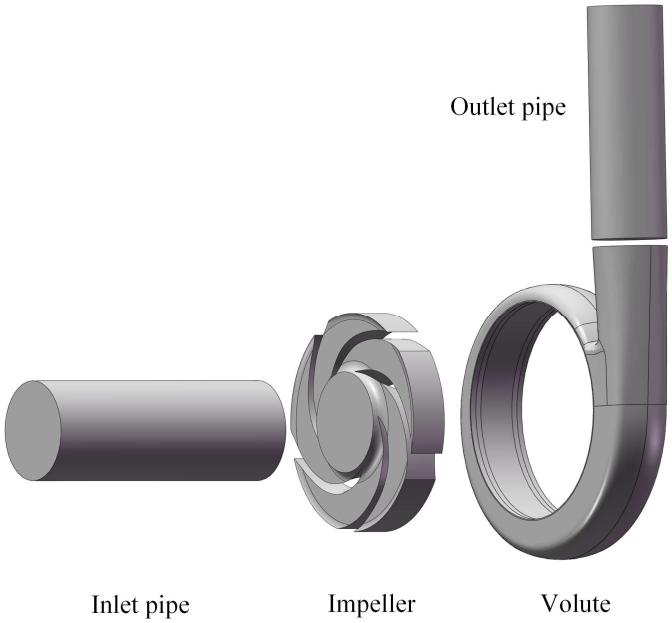

Figure 2. Hydrodynamic model of the fluid domain.

Table 1. Domain dimensions.

Geometric Parameters	Value
Inlet pipe diameter (mm)	350
Length of inlet pipe (mm)	800
Outlet pipe diameter (mm)	260
Length of outlet pipe (mm)	700
Impeller inlet diameter (mm)	350
Impeller outer diameter (mm)	760
Volute outer diameter (mm)	260

Table 2. Mesh type.

Parts	Mesh Type
Inlet pipe	Hexahedral structured mesh
Outlet pipe	Hexahedral structured mesh
Impeller	Tetrahedral unstructured mesh
Volute	Tetrahedral unstructured mesh

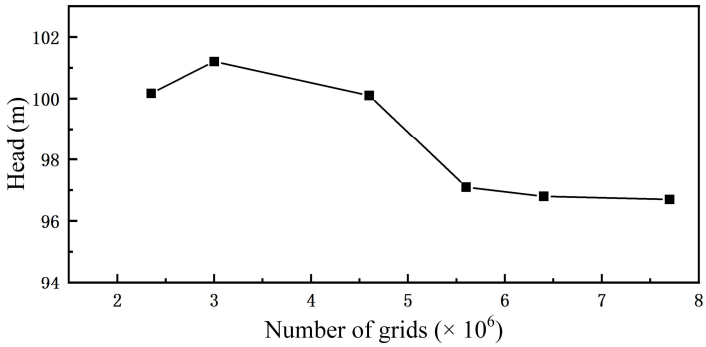

Figure 3. Mesh independence.

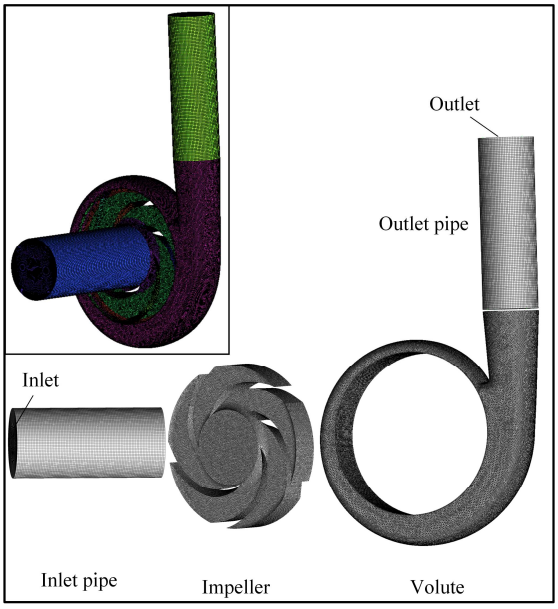

Figure 4. Mesh model.

2.3. Experimental Method

Figure 5 shows the experimental system. Figure 6 shows the comparison of numerical simulation and experimental data for the centrifugal pump under the conditions of a speed of 990 rpm and water as the fluid medium. The flow rates are 220, 509, 715, 970, 1205, and 1347 m^3/h. The numerical simulation adopts the transient calculation mode, and Table 3 shows the specific setup of simulation parameters. It shows that the trend of the two curves of the simulated data and the experimental data is basically the same, with a maximum error of less than 6%. The error between the experiment and the numerical simulation mainly lies in the fact that the numerical calculation ignores the effect of friction during mechanical rotation in the actual use process, and the experimental data are often lower than the numerical simulation data. Comparison results from simulation and experiment show that the calculation method used for centrifugal pumps is appropriate.

Table 3. Parameter settings.

Parameter	Value
Grids	6,454,931
Time step (s)	0.0003367
Turbulence model	RNG k-ε
Inlet velocity (m/s)	0.635, 1.444, 2.02, 2.8, 3.465, 3.9

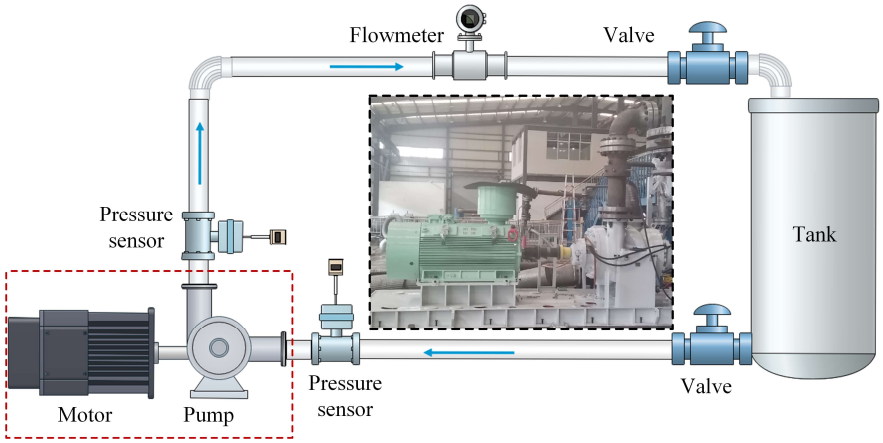

Figure 5. Experimental system.

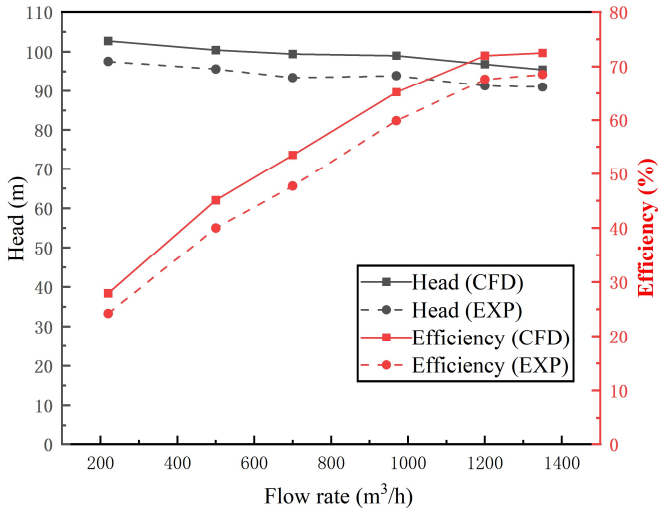

Figure 6. Performance comparison.

2.4. Boundary Condition Setting

A numerical simulation of the solid–liquid two-phase flow of the centrifugal pump was carried out to analyze the influence of the prewhirl on the two-phase flow and wear in the inlet pipe. In this study, the fluid medium was water, the particle material was glass, and the wall material was steel. The simulation parameters of EDEM and FLUENT are shown in Tables 4 and 5.

Table 4. Parameter settings in EDEM.

Parameter	Value
Density of particles (kg/m^3)	2000
Particle diameter (mm)	5
Poisson's ratio of particles	0.3
Shear modulus of particles (Pa)	4.7×10^8
Density of walls (kg/m^3)	7800
Poisson's ratio of walls	0.25
Shear modulus of walls (GPa)	1.96
Mass flow rate of particles (kg/s)	13.3
Time step (s)	3.367×10^{-6}
Rotational speed of impeller (rpm)	990
Velocity of particles (m/s)	3.465

Table 5. Parameter settings in FLUENT.

Parameter	Value
Density of fluid (kg/m^3)	998.2
Viscosity of fluid (kg/(m·s))	0.001003
Rotational speed of impeller (rpm)	990
Turbulence model	RNG k-ε
Convergence criteria (all residuals)	0.001
Boundary condition of inlet	Velocity inlet
Boundary condition of outlet	Outflow
Wall (impeller)	Moving wall
Wall (volute)	Stationary wall
Wall (inlet pipe)	Stationary wall
Wall (outlet pipe)	Stationary wall
Time step (s)	3.367×10^{-4}
Velocity of fluid (m/s)	3.465

3. Results and Discussion

3.1. Analysis of Inlet Pipe Prewhirl Characteristics

Impeller rotation has a direct effect on the flow at the impeller inlet. Figure 7 shows the velocity streamline of the inlet pipe, with Figure 7a showing the overall velocity streamline of the inlet pipe and Figure 7b,c showing the streamline of two mutually perpendicular cross-sections. From the figure, it can be noticed that the flow is very complex in the position close to the impeller inlet, with a clear spiral streamline. In the streamline of the two cross-sections, it can also be found that there are many vortices near the impeller inlet. Therefore, the impeller inlet exhibits the phenomenon of prewhirl.

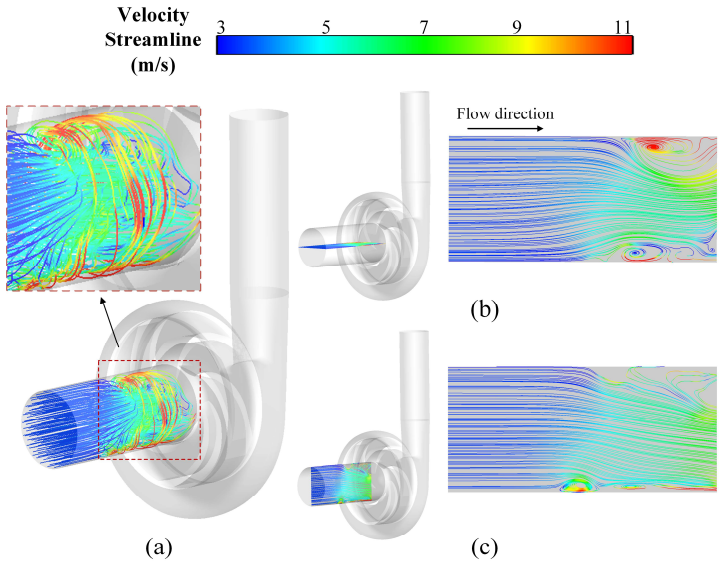

Figure 7. (**a**) The overall velocity streamline of the inlet pipe; (**b**,**c**) The streamline of two mutually perpendicular cross-section.

Figure 8 shows the velocity distribution of the flow at each position of the cross-section of the centrifugal pump inlet pipe, which is divided into a total of 11 cross-sections, and the distance between the 2 neighboring cross-sections is 1 d/D. In the position away from the impeller inlet, the fluid velocity distribution is uniform. The closer to the impeller inlet, the larger the fluid velocity, and in the outermost circle of the cross-section, it will form an obvious high-speed zone. The reason is that the impeller rotation leads to the fluid in the impeller inlet being produced by the prewhirl, and close to the wall of the flow, it will be more intense.

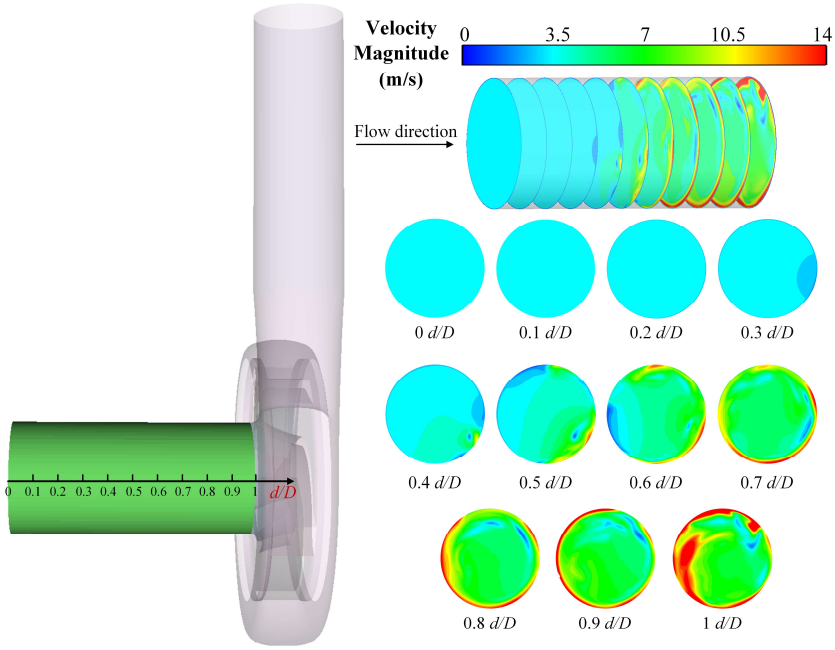

Figure 8. The flow velocity at each position of the cross-section.

To further quantify the fluid velocity magnitude in the cross-section, a radial slice was made at the cross-section of the centrifugal pump inlet pipe, as shown in Figure 9, to analyze the average fluid velocity magnitude at each cross-section along the radial direction. The distribution of radial velocity magnitude along the cross-section of the centrifugal pump inlet pipe is shown in Figure 10. As can be seen from the figure, the velocity magnitude across the inlet pipe remains essentially constant until r/R = 0.8, after which it rises sharply. The largest increase in velocity magnitude occurs between r/R = 0.9 and 1. The dashed box shows the more detailed velocity magnitude distribution in this range. It can be seen that there is a maximum at r/R = 0.98 and a slight decrease in fluid velocity further out on the circumference due to the decelerating effect of the wall on the fluid close to the wall.

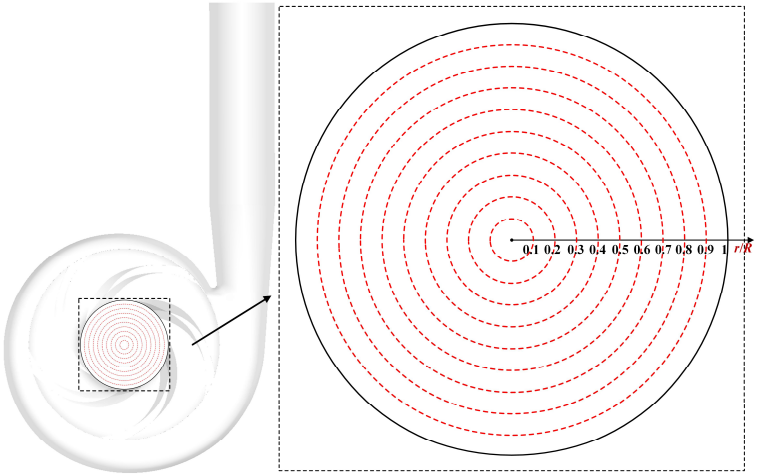

Figure 9. Schematic diagram of inlet pipe division.

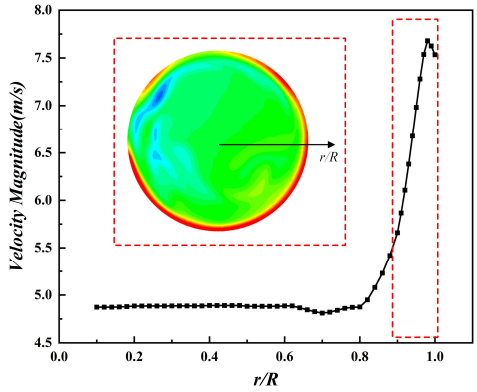

Figure 10. Radial fluid velocity magnitude in cross-section.

3.2. Effect of Prewhirl on Particle Motion

The flow at the impeller inlet directly affects the movement of the particles, which leads to wear. At a particle mass concentration of 13.3 kg/s, Figure 11a shows the distribution of the particles in the whole pump and the graph of the average velocity variation of 50 randomly selected particles among the initially generated particles in the whole centrifugal pump, and Figure 11b shows the particles in the inlet pipe at different times, where the particles generated at 0.2 s are just close to the impeller inlet. From Figure 11a, the particles have a significant velocity enhancement before 0.2 s, but the enhancement is smaller than entering the impeller after 0.2 s. This indicates that the particles are affected by the fluid and accelerated before 0.2 s, i.e., before entering the impeller. The acceleration of the fluid on the particles here is caused by the prewhirl of the impeller inlet, which appears to be a rotational reverse flow, pulling the particles to produce a velocity different from the direction of the initial velocity of the particles, resulting in an increase in the velocity of the particles. The particles entering from the impeller inlet are accelerated to a very high value by the high-speed rotating impeller, and then the particles are thrown out of the impeller and collide with the volute, resulting in a sharp decrease in velocity. Figure 11b shows the initially generated particles from the inlet pipe just approaching the impeller inlet being influenced by the flow to change their state of motion. With the change in time, the particles in the middle part of the inlet pipe are obviously piled up due to the rotational reverse flow. There exists a circle of particles with lower velocities, and the particles on the right side are accelerated to a higher state. At the same time, near the inlet of the impeller, there will be a clear "fewer-particle zone" at the top and bottom sides of the pipe. The distribution of the particles will become uneven. Figure 12 shows the distribution of particles in the impeller inlet cross-section at different moments. Figure 12 confirms that the distribution of particles at the impeller inlet is not uniform and that a "fewer-particle zone" in the shape of a circle is formed in the circular cross-section close to the outer circumference, creating an uneven flow of particles.

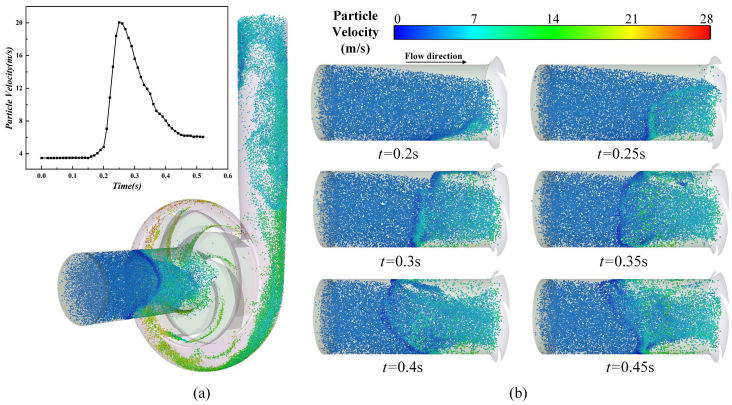

Figure 11. (**a**) The distribution of the particles in the whole pump and the average velocity variation of particles; (**b**) The particles in the inlet pipe at different times.

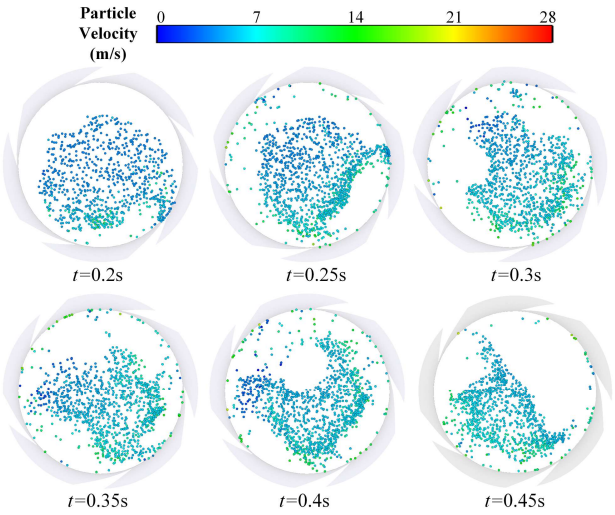

Figure 12. Distribution of particles in the impeller inlet cross-section.

Figure 13 shows the fluid force on the particles at the inlet pipe as well as the average magnitude of the fluid force on the particles in each region. From the figure, it can be seen that the particles at the position farther away from the impeller inlet are almost not subjected to the fluid force because the velocity of the particles here is consistent with the flow. While the direction of motion of the subsequent particles is changed, the fluid force on the particles becomes larger, which proves that it is the change in the flow that leads to the change in the state of motion of the particles. The particles with a higher velocity of the inlet pipe in Figure 11b also correspond exactly to the particles with a higher fluid force in Figure 13. It can also be noticed from Figure 13 that the particles about to enter the impeller inlet are subjected to a great fluid force because the fluid velocity here has been accelerated to a higher value by the impeller, which creates a large velocity difference with the particles, thus creating a stronger traction effect.

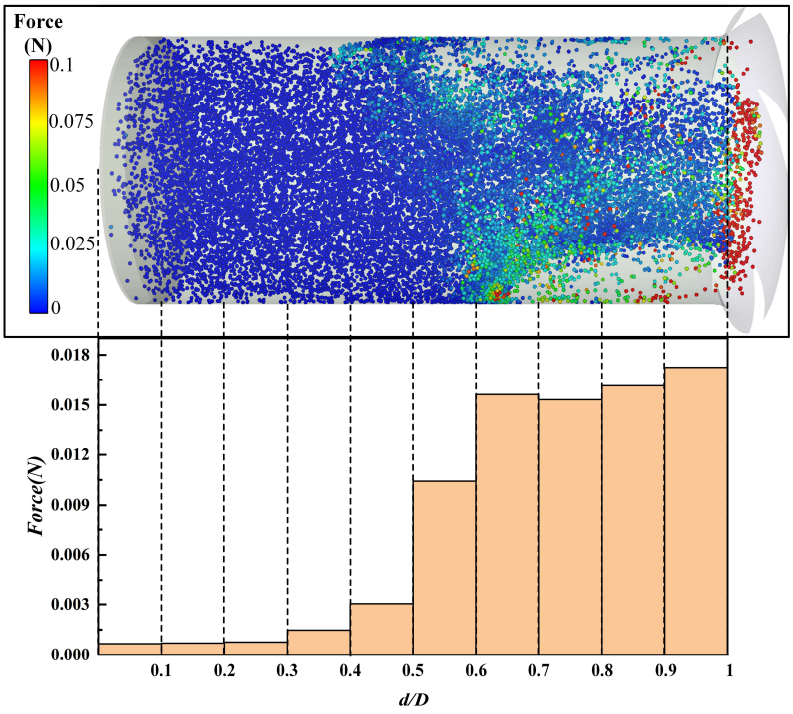

Figure 13. Fluid forces on particles.

3.3. Effect of Prewhirl on Inlet Pipe Wear

Figure 14 shows the wear of the centrifugal pump inlet pipe at 0.6 s at a particle mass flow rate of 13.3 kg/s, with view A being an elevation view and view B being a top view. From the figure, it can be seen that the wear distribution is not uniform. The half of the pipe away from the impeller inlet is hardly subjected to wear by the particles, and the wear is almost concentrated on the half of the pipe close to the impeller. The region of high wear is also unique, showing a triangle. The boundary of the high-wear region moves from the interface between the inlet pipe and the impeller inlet along the inner wall of the pipe towards the middle of the inlet pipe. This corresponds to the change in the motion of the particles in Figure 11b, where a change in the flow leads to a change in the motion of the particles, which ultimately results in varying degrees of wear on the inlet pipe.

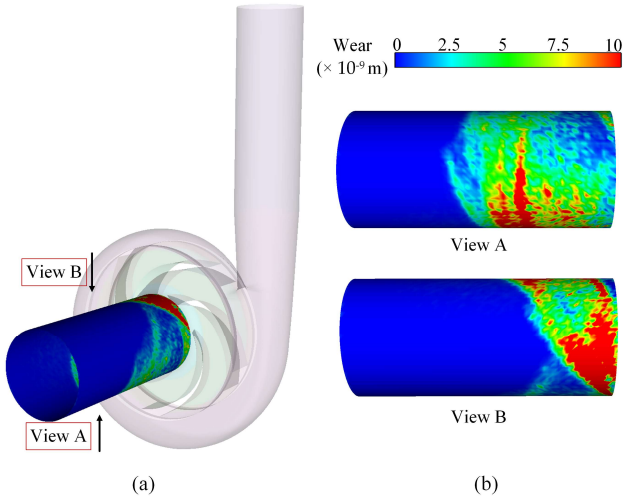

Figure 14. (**a**) Wear of centrifugal pump inlet pipe; (**b**) The elevation view and the top view.

In order to obtain a clearer picture of the degree of wear in each region of the inlet pipe, the half portion near the impeller inlet (i.e., 0.5 *d/D* to 1 *d/D*) is now divided into 40 regions, as shown in Figure 15. The pipe is divided into symmetrical sections on the left and right sides, which are cropped and unfolded along the position of the dotted line. The 40 regions were analyzed for average wear, and the results are shown in Figure 16, where the dashed box shows the 2D unfolding. From the figure, it can be seen that the high-wear regions are mainly distributed in the three regions of L4, L9, and L13, indicating that the stacked particles have more impacts in these regions. Meanwhile, from the two-dimensional unfolding diagram, it can be clearly seen that there is a clear intersection line between the high-wear region and the low-wear region, which is consistent with the results shown in Figure 14. The high-wear areas show a nearly triangular shape, while the low-wear areas show a banded distribution.

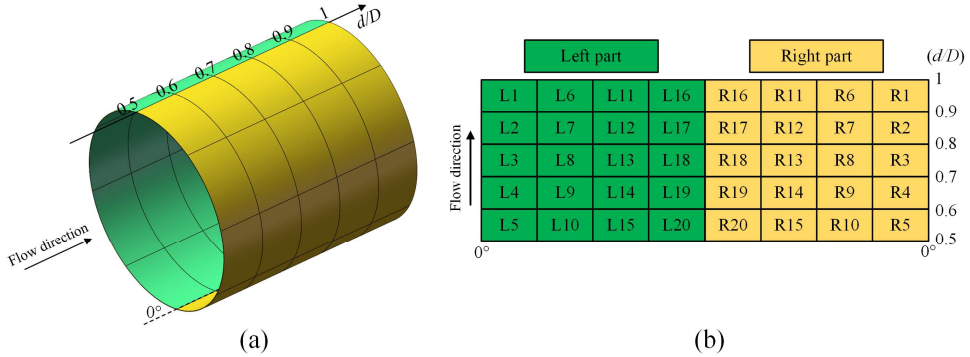

Figure 15. (**a**) Schematic diagram of inlet pipe division; (**b**) Schematic diagram of unfolded pipe.

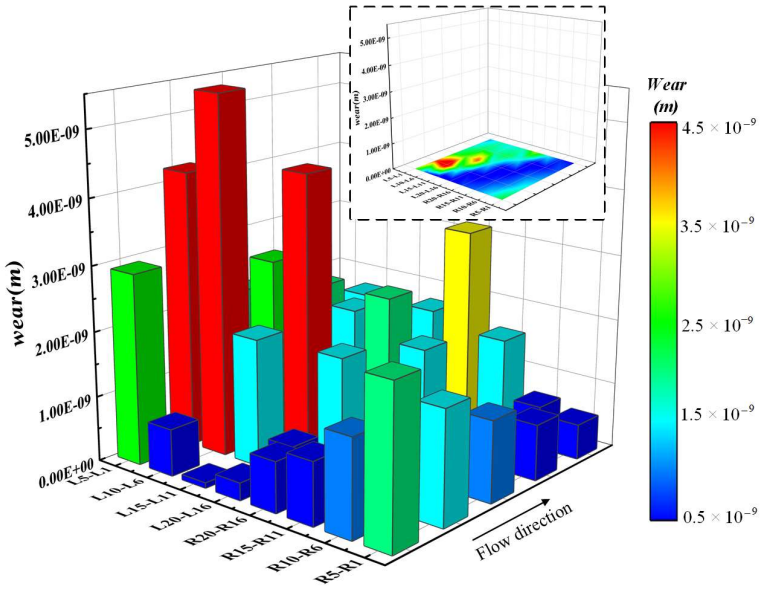

Figure 16. Amount of wear in different regions.

Figure 17 shows the cumulative force of particles on the wall surface for the 40 regions, and the cumulative force includes tangential and normal cumulative forces. From the figure, it can be seen that the regions with high cumulative forces are almost the same as the regions with high wear in Figure 16, which are also mainly distributed in the three regions of L4, L9, and L13. This indicates that the cumulative force has a great influence on the wall wear. It can also be found that the change trend of tangential cumulative force and normal cumulative force is consistent, but the tangential cumulative force is much larger than the normal cumulative force in almost every region. This indicates that the main cause of wall wear is the tangential cumulative force.

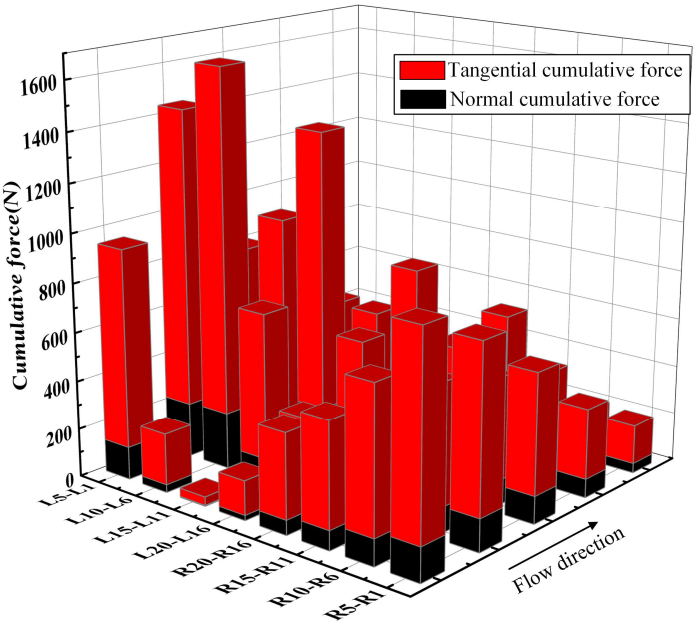

Figure 17. Magnitude of cumulative forces in different regions.

Figure 18 shows the number of particle–wall collisions, maximum energy loss and average energy loss in a collision, and average wear over time for the entire inlet pipe. The number of particle–wall collisions has been increasing overall, indicating that the particle

accumulation in the inlet pipe has not been alleviated, and there are still many particles that have been in contact with the inlet pipe wall. The maximum energy loss of a single collision starts to rise around 0.2 s due to the acceleration of the prewhirl flow and fluctuates after 0.3 s, but it always floats up and down within a range. The maximum energy loss of a single collision has a peak at about 0.05 s, which takes place because most of the collisions occurring at this time are the first collisions of particles with the wall. With the change in time, many collisions will be multiple collisions of particles with the wall, and the loss of collision energy will be smaller. The maximum energy loss for a single collision of particles starts to increase around 0.2 s, while the same fluctuates within a range after 0.3 s. Although the collision of particles with the wall has been increasing before 0.2 s, the average wear of the inlet pipe is almost 0 because the average energy loss of the collision is small. The average wear of the wall has been increasing until after 0.2 s because not only the number of collisions is increasing at this time but also the average energy loss of the collision. The wear amount will keep increasing with time.

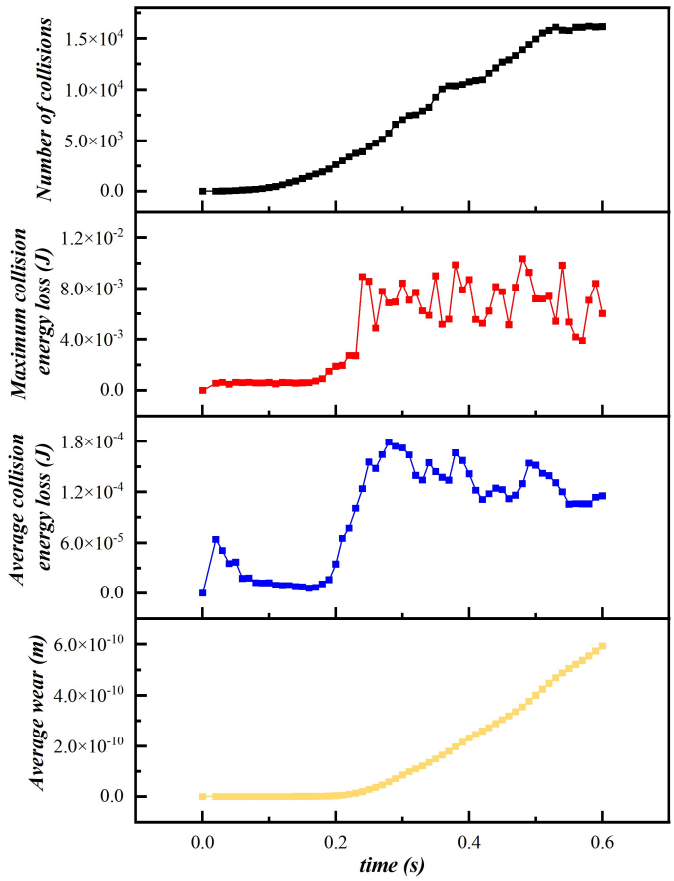

Figure 18. Average wear rate, number of collisions, and energy loss.

4. Conclusions

The prewhirl at the impeller inlet causes changes in the fluid and particles, which affects the wear of the inlet pipe. Therefore, in this paper, based on the CFD-DEM method, a solid–liquid two-phase numerical simulation of a centrifugal pump with a flow rate of 1200 m^3/h is carried out to study the particle motion and wear of the inlet pipe. The main research content and conclusions are summarized as follows:

1. Impeller rotation causes a change in the flow field at the inlet of the impeller, producing a pronounced helical velocity streamline. The velocity of the fluid will increase in the radial direction along the inlet pipe cross-section and will rise sharply after r/R = 0.8, reaching a maximum value at r/R = 0.98.

2. Prewhirl causes the particle motion at the impeller inlet to be affected, and the particles are pulled by the flow and subjected to increased fluid forces and increased velocity. Near the impeller inlet, the average fluid force on the particles is between 0.015 and 0.018 N. At the same time, the effect of rotational reverse flow can lead to an uneven distribution of particles and the existence of accumulation in the middle part of the inlet pipe.
3. Prewhirl leads to a change in the state of motion of the particles and thus affects the wear distribution in the inlet pipe. The high-wear regions of the inlet pipe are L4, L9, and L13 and show a triangular shape, while the low-wear regions show a band structure. The cumulative force of particles on the wall surface has a high impact on wear, while the tangential cumulative force is a more influential factor. Prewhirl leads to an increase in both the maximum and average energy loss per collision, which affects the wear of the inlet pipe.

In this paper, mainly the effect of prewhirl on the particle motion and wear of the inlet pipe is investigated. Subsequently, taking into account the coupling system of the piping and the centrifugal pumps, the effect of prewhirl on the particles, flow field, and external characteristics inside the system will be analyzed. This aspect can be explored further in the future.

Author Contributions: Conceptualization, Y.L. and J.C.; methodology, J.C.; software, Y.Z.; validation, X.C. and W.L.; formal analysis, Y.L.; investigation, X.C. and W.L.; resources, X.C. and W.L.; data curation, Y.Z.; writing—original draft preparation, J.C.; writing—review and editing, Y.L.; visualization, X.C.; supervision, W.L.; project administration, Y.L.; funding acquisition, Y.L. All authors have read and agreed to the published version of the manuscript.

Funding: This work was supported by the National Key R&D Program of China (Grant No. 2022YFE0126600) and the Key Research and Development Program of Zhejiang Province (Grant No. 2022C01194).

Institutional Review Board Statement: Not applicable.

Informed Consent Statement: Not applicable.

Data Availability Statement: The data presented in this study are available on request from the corresponding author. Due to the huge amount of data, it is not convenient to save at publicly archived datasets.

Conflicts of Interest: Authors Xing Chen and Wenjin Li were employed by the company Kunming Jiahe Science & Technology Co., Ltd., Yuhai Zheng was employed by the company Zhejiang Institute of Mechanical & Electrical Engineering, Co., Ltd. The remaining authors declare that the research was conducted in the absence of any commercial or financial relationships that could be construed as a potential conflict of interest.

Nomenclature

f_{fp}	momentum exchange
k	turbulent kinetic energy
ε	dissipation rate
G_k	turbulent kinetic energy due to the mean velocity gradient
μ	kinetic viscosity coefficient
μ_t	turbulent viscosity coefficient
σ_k	Prandtl numbers corresponding to k
σ_ε	Prandtl numbers corresponding to ε
m_p	mass
V_p	velocity of the particle
$\sum F_c$	sum of all contact forces
F_g	force of gravity
F_f	force of fluid
I_p	particle rotational inertia
M_{ct}	sum of the contact momentum of the particle with other particles

ω_p	angular velocity
M_{fp}	moment of resistance
F_d	fluid resistance
F_l	lift force
F_B	Basset force
F_{am}	added mass force
F_p	pressure gradient force

References

1. Wu, X.; Su, P.; Wu, J.; Zhang, Y.; Wang, B. Research on the Relationship between Sediment Concentration and Centrifugal Pump Performance Parameters Based on CFD Mixture Model. *Energies* **2022**, *15*, 7228. [CrossRef]
2. Li, Y.; Zhu, Z.; He, W.; He, Z. Numerical Simulation and Experimental Research on the Influence of Solid-phase Characteristics on Centrifugal Pump Performance. *Chin. J. Mech. Eng.* **2012**, *25*, 1184–1189. [CrossRef]
3. Cui, B.; Shi, M. Analysis of Unsteady Flow Characteristics Near the Cutwater by Cutting Impeller Hub in a High-Speed Centrifugal Pump. *J. Mar. Sci. Eng.* **2024**, *12*, 587. [CrossRef]
4. Yin, J.; Li, J.; Chen, H.; Hu, Y.; Wang, D. Investigation on the Backflow Induced Pre-Rotation of RCP. In Proceedings of the 2014 22nd International Conference on Nuclear Engineering, Prague, Czech Republic, 7–11 July 2014; Volume 45899, p. V001T01A018.
5. Chalghoum, I.; Elaoud, S. Transient Analysis of the Dynamic Flow Characteristics of the Centrifugal Pump at Different Operating Points. *Nav. Eng. J.* **2019**, *131*, 113–122.
6. Zhou, C.M.; Wang, H.M.; Huang, X.; Lin, H. Influence of the positive prewhirl on the performance of centrifugal pumps with different airfoils. conference series: Earth and environmental science. *IOP Conf. Ser. Earth Environ. Sci.* **2012**, *15*, 032020.
7. Huang, R.; Ye, W.; Dai, Y.; Luo, X.; Wang, Y.; Du, T.; Huang, C. Investigations into the unsteady internal flow characteristics for a waterjet propulsion system at different cruising speeds. *Ocean Eng.* **2020**, *203*, 107218. [CrossRef]
8. Lu, J.; Liu, X.; Zeng, Y.; Zhu, B.; Hu, B.; Hua, H. Investigation of the noise induced by unstable flow in a centrifugal pump. *Energies* **2020**, *13*, 589. [CrossRef]
9. Yang, Y.; Chen, X.; Su, D.; Gu, T.; Xi, B.; Wang, H.; Jiao, W.; Ji, L.; He, Z.; Wang, C. Investigations on the Energy Characteristics and Internal Flow Dynamics of a Mixed-Flow Pump Considering of Inlet Pre-Rotation at Off-Rated Flow Conditions. *Iran. J. Sci. Technol. Trans. Mech. Eng.* **2024**. [CrossRef]
10. Cao, W.; Wang, H.; Tang, J. Study on Wear Characteristics of a Guide Vane Centrifugal Pump Based on CFD–DEM. *J. Mar. Sci. Eng.* **2024**, *12*, 593. [CrossRef]
11. Bandi, S.; Banka, J.; Kumar, A.; Rai, A.K. Effects of sediment properties on abrasive erosion of a centrifugal pump. *Chem. Eng. Sci.* **2023**, *277*, 118873. [CrossRef]
12. Wang, Z.; Qian, Z. Effects of Concentration and Size of Silt Particles on the Performance of a Double-suction Centrifugal Pump. *Energy* **2017**, *123*, 36–46. [CrossRef]
13. Deng, L.; Lu, H.; Liu, S.; Hu, Q.; Yang, J.; Kang, Y.; Sun, P. Particle anti-accumulation design at impeller suction of deep-sea mining pump and evaluation by CFD-DEM simulation. *Ocean Eng.* **2023**, *279*, 114598. [CrossRef]
14. Hu, Q.; Chen, J.; Deng, L.; Kang, Y.; Liu, S. CFD-DEM simulation of backflow blockage of deep-sea multistage pump. *J. Mar. Sci. Eng.* **2021**, *9*, 987. [CrossRef]
15. Chung, J.S.; Tsurusaki, K. Advance in deep-ocean mining systems research. In Proceedings of the International Ocean and Polar Engineering Conference, ISOPE, Osaka, Japan, 10–15 April 1994. ISOPE-I-94-003.
16. Zou, W. COMRA's research on lifting motor pump. In Proceedings of the Ocean Mining and Gas Hydrates Symposium, ISOPE, Lisbon, Portugal, 1–6 July 2007. ISOPE-M-07-032.
17. Li, Y.; Cao, J.; Xie, C. Research on the Wear Characteristics of a Bend Pipe with a Bump Based on the Coupled CFD-DEM. *J. Mar. Sci. Eng.* **2021**, *9*, 672. [CrossRef]
18. Li, Y.; Xiao, J.; Lin, Z.; Zhu, Z. Two-phase flow and wear of 90° bend pipes by normally distributed particles. *Proc. Inst. Mech. Eng. Part E J. Process Mech. Eng.* **2023**. [CrossRef]
19. Tang, C.; Yang, Y.C.; Liu, P.Z.; Kim, Y.J. Prediction of abrasive and impact wear due to multi-shaped particles in a centrifugal pump via CFD-DEM coupling method. *Energies* **2021**, *14*, 2391. [CrossRef]
20. Shi, X.; Ding, W.; Xu, C.; Xie, F.; Tian, Z. Numerical investigation of inlet section structure effect on wear characteristic of particle condition in centrifugal slurry pump by CFD-DEM coupling. *Part. Sci. Technol.* **2023**, *41*, 834–843. [CrossRef]
21. Su, X.; Tang, Z.; Li, Y.; Zhu, Z.; Mianowicz, K.; Balaz, P. Research of particle motion in a two-stage slurry transport pump for deep-ocean mining by the CFD-DEM method. *Energies* **2020**, *13*, 6711. [CrossRef]
22. Tan, M.; Shao, C.; Wu, X.; Liu, H.; Pan, B. Numerical study on cylindrical particle solid–liquid two-phase flow in a slurry pump. *Comput. Part. Mech.* **2023**. [CrossRef]
23. Wang, R.; Guan, Y.; Jin, X.; Tang, Z.; Zhu, Z.; Su, X. Impact of particle sizes on flow characteristics of slurry pump for deep-sea mining. *Shock. Vib.* **2021**, *2021*, 6684944. [CrossRef]
24. Li, Y.; Liu, D.; Cui, B.; Lin, Z.; Zheng, Y.; Ishnazarov, O. Studying particle transport characteristics in centrifugal pumps under external vibration using CFD-DEM simulation. *Ocean Eng.* **2024**, *301*, 117538. [CrossRef]
25. Victor, Y.; Steven, A.O. Renormalization group analysis of turbulence. I. Basic theory. *J. Sci. Comput.* **1986**, *1*, 3–51.

26. Cundall, P.A.; Strack, O.D.L. A discrete numerical model for granular assemblies. *Géotechnique* **1979**, *29*, 47–65. [CrossRef]
27. Archard, J.F. Contact and Rubbing of Flat Surfaces. *J. Appl. Phys.* **1953**, *24*, 981–988. [CrossRef]